3rd National Level Students' Research Conference on "Innovative Ideas and Inventions in Computer Science & IT with Its Sustainability"
In association withInternational Journal of Scientific Research in Computer Science, Engineering and Information Technology | ISSN : 2456-3307 (www.ijsrcseit.com)

Alunite (Soil) Mineral Identification in Aurangabad District

Jaypalsing N. Kayte, Ratnadeep R. Deshmukh
Department of Computer Science & IT, Dr. Babasaheb Ambedkar Marathwada University, Aurangabad, Maharashtra, India

ABSTRACT

This paper us an analysis of hyperspectral image spectra (Hyperion EO-1) and field spectra (Fieldspec4) data to identify mineralization zone and mineral spectral behavior. Comparative analysis of field spectra and image spectra is very useful to identify mineralization zone and surrounding host rocks and soil. The chosen method entails collecting field spectra, processing them for noise, and spectral matching with USGS library end-members. A Hyperspectral remote sensing technique was applied with three progressive steps. First, the processing and interpretation of space-borne Hyperion (EO-1) data with a focus on the areas characterized by alteration and mineralized zones. Preliminary processing of Hyperion (EO-1) data involved removal of striping followed by atmospheric corrections. Additional processing stages include the Minimum Noise Fraction (MNF) transformation to minimize data dimensionality and the Pixel Purity Index (PPI) as a pure pixel locator. The Spectral Angle Mapper (SAM) categorization technique aids in the detection of end members. According to this study, the probability of alunite mineral is 0.85.

Keywords— PPI, SAM, EO-1, MNF, USGS, IMA, FLAASH, VNIR, SWIR, DN, CCD, PCA, NASA, BE, SFF

I. INTRODUCTION

Mineral deposits are geological entities found deep under the earth's crust that contain unusually high concentrations of certain elements with economic worth. The polarity of tectonic magmatic domains established by crustal evolutionary processes and produced by favorable surficial habitats and processes influence the homogeneity of concentrations in the earth's crust.Many developing countries rely on the mining of their natural resources to keep their economies afloat. Mineral exploration and exploitation, particularly of metalliferous deposits, is critical for many developing countries. Finding new mineral deposits, particularly metalliferous resources, will thus be beneficial to a country's economic development. In turn, reliable geo-information in the form of geological and mineral prospecting maps is critical for mineral resource exploration and development. However, geological and mineral exploration methods necessitate large sums of money, a long period, and a lot of human work, especially in difficult-to-reach places. When compared to multispectral remote sensing, hyperspectral (Hyperion EO-1) remote sensing has a greater number of bands. It is possible to apply the vast quantity of spectrum information to a variety of applications such as monitoring, agriculture, pollution, landuse / landcover, soil and water quality monitoring, mineral identification, food quality monitoring, and so on. L. Zhang and B. Du (2012). A mineral is a natural substance with a chemical formula that is frequently solid, inorganic, and has a crystal structure. The International Mineralogical Association (IMA) has accepted 5,070 minerals out of 5,300 known minerals. Schneider, S., Murphy, R. J., and Melkumyan, A. (2014). Aluminium phosphates and sulphates of the alunite super group (APS minerals) are found in a variety of formation settings including metamorphic, igneous, and sedimentary worlds. Alunite is a mineral that forms when acidic, typically ore-bearing, solutions modify orthoclase feldspar-rich rocks. H. G. Dill (2001). However, even if geology or ground truth information is inadequate, mineral discovery or research is achievable with the aid of remote sensing. As a result, it would be a strong instrument for cost-effective mineral examination, which would substantially aid in the improvement of the country's economy. Geologists and others must prospect for mineral resources in remote places. R. Gore, A. Mishra, and R. Deshmukh (2020). Figure 1 depicts the mineral alunite and its field spectrum. To process the hyperspectral data, the following steps are taken: elimination of poor bands, removal of vertical strips in pictures, radiometric calibration, FLAASH atmospheric adjustment, minimal noise percentage, and pixel quality index. Finally, the EO Hyperion data was classified using the Spectral Angle Mapper (SAM) classification method.

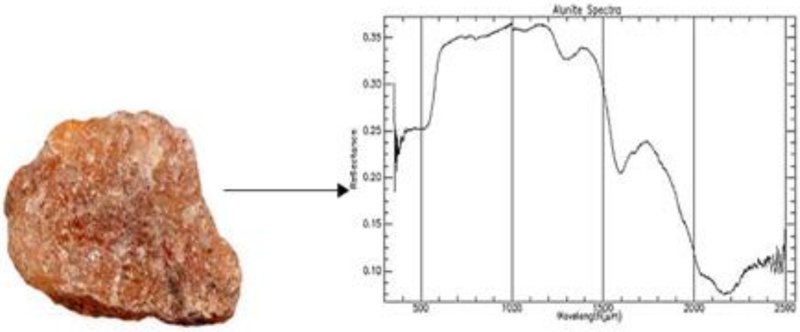

FIGURE. 1. THE SPECTRAL PATTERN OF ALUNITE MINERAL

II. STUDY AREA

Aurangabad District is one of the 36 districts of the state of Maharashtra in western India. In Aurangabad district mineral mapping report is not mentioned as government contribute mineral mapping report in India in general The most significant metallic and non-metallic minerals found in the Aurangabad district, such as Alunite, iron ore, and clay, are used in a variety of industries.

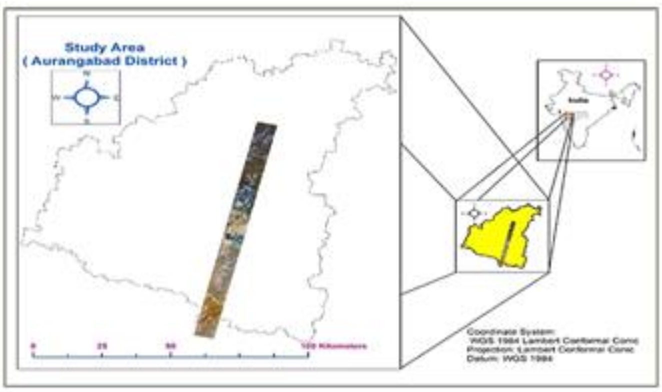

FIGURE. 2. THE RESEARCH STUDY AREA GEOLOGICAL POSITION.

A. Geological Information

The Aurangabad District, which is located on the Deccan plateau, is surrounded by the Deccan Traps, which formed during the Late Cretaceous and Lower Eocene periods. Thin alluvial deposits above the Deccan Traps run parallel to the main rivers. The basaltic lava flows of the Deccan Traps are the district's sole significant geological formation. The lava flows are horizontal, with each flow consisting of two layers. The top layer is made up of vesicular and amygdule zeolitic basalt, whereas the lower layer is made up of massive basalt Mahoney, J. J. (1988).

B. Hyperion (EO-1)

Data is utilised to identify the Alunite mineral in the present research Hyperion (EO-1). Hyperion (EO-1) is a US spacecraft with 242 spectral bands ranging from 0.4 to 2.5m, calibrated at 10nm intervals, and calibrated in 16-bit radiometric resolution. The width of the swath is 7.2km, and the height is 705km. It has a spatial resolution of 30m and a revisit period of 16 days. E. M. Middleton et al (2013). Imagery from the Hyperion (EO-1) scanner requires suitable preprocessing processes such as poor band removal, ertical strip removal, converting DN data to radiance values, atmospheric adjustment such as FLAASH, QUAC, and so on. M. Vigneshkumar and K. Yarakkula (2017). The metadata information for the hyperspectral data is shown in Table 1. The Hyperion (EO-1) visible and VNIR area (0.4 – 1.2m) from band 1 to band 70, which is mostly utilised for vegetation mapping. Hyperion (EO-1) SWIR (1.2-2.5m) from band 71 to band 224. Due to the lack of illumination and sensor overlap, only 198 of the 242 bands have been calibrated Upadhyay, M. R. (2013). The geological position of the research region is depicted in Figure 2.

TABLE I. DOWNDOADED HYPERION (EO-I) DATA METAFILE INFORMATION

Data Set Attribute	Attribute Value
Entity ID	EO1H1460462015358110Kv
Acquisition Data	2015-12-24
Reference_Datum	WGS84
Scene Start Time	2015 358 03:42:21
Scene Stop Time	2015 358 03:46:40
SUN_AZIMUTH	130.250063
Satellite Inclination	26.048956
SENSOR_LOOK_ANGLE	7.8141
IMAGE_UL_CORNER_LAT	20.311958
IMAGE_UL_CORNER_LON	75.405204
IMAGE_UR_CORNER_LAT	20.298772
IMAGE_UR_CORNER_LON	75.475783
IMAGE_LL_CORNER_LAT	19.393001
IMAGE_LL_CORNER_LON	75.193376
IMAGE_LR_CORNER_LAT	19.379903
IMAGE_LR_CORNER_LON	75.263570
PRODUCT_UL_CORNER_LAT	20.315440
PRODUCT_UL_CORNER_LON	75.190621

PRODUCT_UR_CORNER_LAT	20.314891
PRODUCT_UR_CORNER_LON	75.477985
PRODUCT_LL_CORNER_LAT	19.377421
PRODUCT_LL_CORNER_LON	75.189505
PRODUCT_LR_CORNER_LAT	19.376899
PRODUCT_LR_CORNER_LON	75.475186

III. METHODOLOGY

Several preprocessing procedures are necessary to categorise the hyperspectral data. Figure 3 depicts the detailed methods used to analyse the Hyperion (EO-1) data.

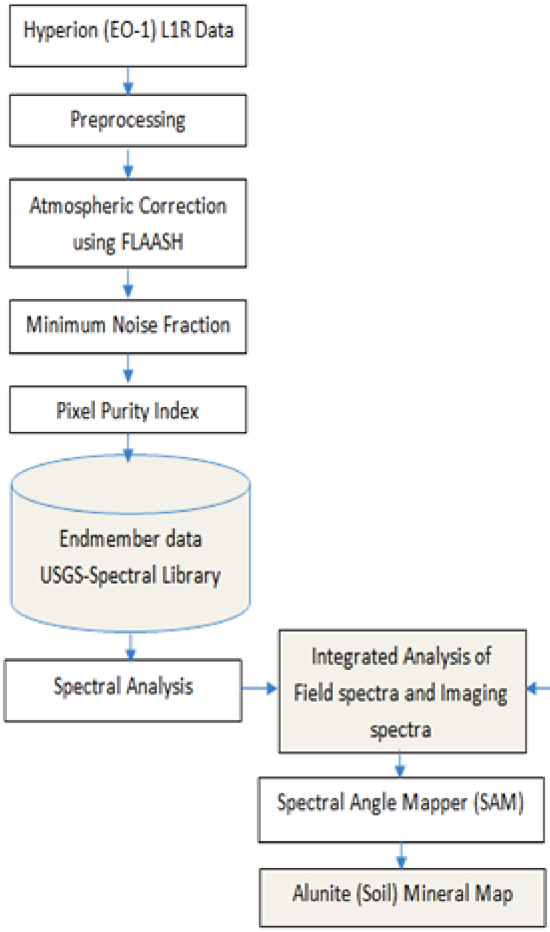

FIGURE. 3. ALUNITE SOIL MINERAL MAPPING METHODOLOGY

A. Remove the zero bands and bad bands

The Hyperion (EO-1) image comprises pixels with no information, which are referred to as zero bands. They may be found in bands 1-7, 58-76, and 225-242. M. R. Upadhyay (2013). In the spectral area, bad bands have a lot of noise and water vapour. It varies depending on the location and scanning time for each image. F. Van Der Meer (2004).

B. Remove the vertical stripe in the imagery

The number of vertical strips in a push-broom scanner's column. The raw image has numerous dark and bright columns due to a change in calibration or the failure of some detectors in the CCD display at the time of imprisoning the image. Check for column dropout or band issues before applying atmospheric adjustments. The terrible columns are substituted by averaging the preceding and next columns. M. K. Pal and A. Porwal (2015). To remove the strips in this study, a local destriping method is utilised.

$$\sum_{j=1}^{n} \frac{\left(x_{i-1,j,k}\right) + \left(x_{j+1,j,k}\right)}{2n} \qquad 1$$

The equation 1 shows the local destriping algorithm.

C. Radiometric Calibration

The amount of light energy measured by the sensor from the item being viewed is referred to as radiance. C. Arellano, C. Wyatt (2012). When distributing remote sensing data, radiometric calibration is employed. It comprises adjustments for the distant sensor's sensitivity, topography and sun angle, as well as air scattering and absorption. It is most often used to transform a digital number to a radiance value for each pixel. It is available in three different formats: BIL, BSQ, and BIP.

D. Fast Line of sight Atmospheric Analysis of Hypercube (FLAASH)

FLAASH corrects wavelengths in the VNIR and SWIR ranges up to 3m. FLAASH has features such as adjacency correction to calculate a scene-average visibility, cirrus and opaque cloud map, and modifiable spectral shine for artefact suppression. H. G. Solutions (2017).

E. Minimum noise fraction (MNF)

To minimise the complexity of hyperspectral data, MNF was developed as an alternative to principle component analysis. It is distinguished by a two-pace cascaded PCA. The first stage is to use a probable noise covariance matrix to decorrelate and rescale the data noise; it has item discrepancy and no band-to-band correlations. In the second pace, a standard PCA of noise-whitened data is employedIt splits the data space into two sections: big Eigen Values and rational Eigen pictures, and small Eigen Values and noise-conquered images. In further processing, the noise is removed from the data by employing just the logical sections, therefore humanising the spectrum processing effects. B. Datt (2003).

F. Pixel Purity Index (PPI)

Vigneshkumar, M., and Yarakkula, K. manipulate the pixel purity index algorithm for each pixel in the picture cube by randomly generating appearance in the N-dimensional, a distributed scheme of the MNF converted information (2017). Total points in the space are now divided into lines, and those that go down at the lines' extremities are computed. Individual pixels that count above a certain threshold are labelled "pure" after repeated projections to different lines.

G. Spectral Analysis

The categorization of materials based on their spectral distinctiveness is aided by spectral analysis. To rank the equivalent of an image spectrum to the minerals in a spectral library, the spectral analysis utilises a number of approaches, including binary encoding, spectral angle mapping, and spectral feature fitting. M. Vigneshkumar and K. Yarakkula (2017).

H. Spectral Angle Mapper

SAM computes the angular distance in n dimensions between an image's reflection spectrum and the mineral spectral. The categorised picture gives the best SAM match at each pixel for each end member based on the angular distance in radians between the image spectrum and the reference spectrum. The spectral angles with fewer spectral angles are represented by darker pixels, and the spectra are parallel to the reference spectrum. By changing the thresholds used to choose the pixels in the SAM image, the rule images may be utilised for classification. M. R. Upadhyay (2013).

IV. RESULT AND DISCUSSION

A. Removing the bad bands from Hyperion (EO-1) data

The Hyperion (EO-1) data set has 242 bands, 120 of which are calibrated; the other bands are affected by noise, non-illuminated, and water vapour. The list of underused and poor bands of the Hyperion (EO-1) sensor is shown in Table 2. Figure 4 clearly depicts the overlap zone of zero bands. Figure 5 depicts the spectral profile plot after the zero bands and overlap region have been removed. Figures 5 and 5 demonstrate the effect of eliminating problematic bands from the spectral profile plot.

TABLE II. FOR SUBSET DATA THE PARAMETERS FOR FLAASH ARE:

Parameter	**Characteristics**	**Remarks**
Latitude		Central Latitude
Longitude		Central Longitude
Sensor Type	Hyperion (EO-1)	Hyper Spectral Sensor
Ground Elevation	0.38km / 380m	220m for the Subset Area
Pixel Size	30m	Spatial Resolution of Hyperion (EO-1) Sensor is 30M.
Flight Date	29/09/2015	Date of Acquisition
Flight Time	03:42:21	Average of the Start time and end time.
Atmospheric Model	Mid-Latitude Summer	Depending upon the latitude and the surface temperature of the area the atmospheric model is chosen. It is Mid-Latitude Summer for the Subset Data
Aerosol Model	Near to Urban	Since Subset is an urban + rural area
Water retrieval	Yes	This method is used for retrieving the water amount for each pixel
Water Absorption	1135m	In the Hyperion (EO-1) data of subset data the bandwidth of band 99 ranges from 1134-3796
Initial visibility	40	Because the data was captured in the month of nova and hence the data has naze
Aerosol Retrieval	None (Since the initial visibility is	This method is used for retrieving the aerosol amount and estimating a scene average visibility

	40)	
Spectral polishing	Yes	Spectral polishing done to get smooth reflectance curves.
Wavelength Calibration	No	This method is use for Identifying and correcting wavelength, miscallibaration hyperon sensor are automatically supported for wavelength recalibration.

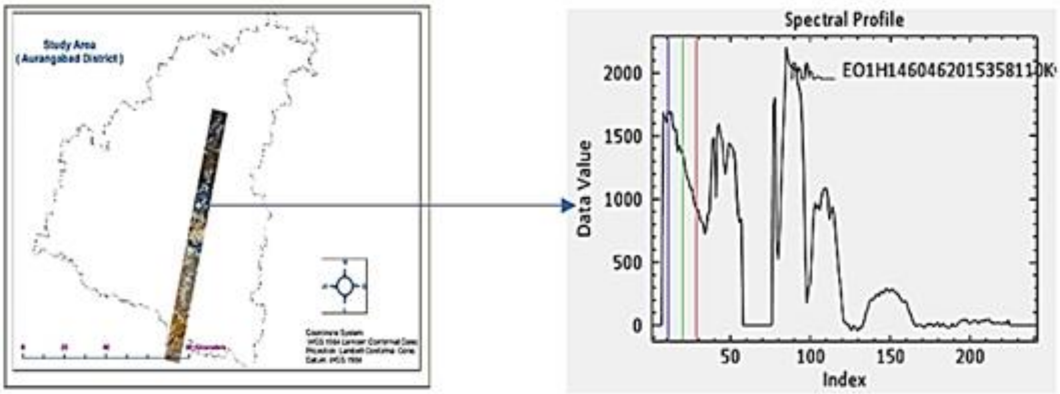

FIGURE. 4. PRIOR TO THE REMOVAL OF THE BAND BANDS AND THE SPECTRAL PLOT

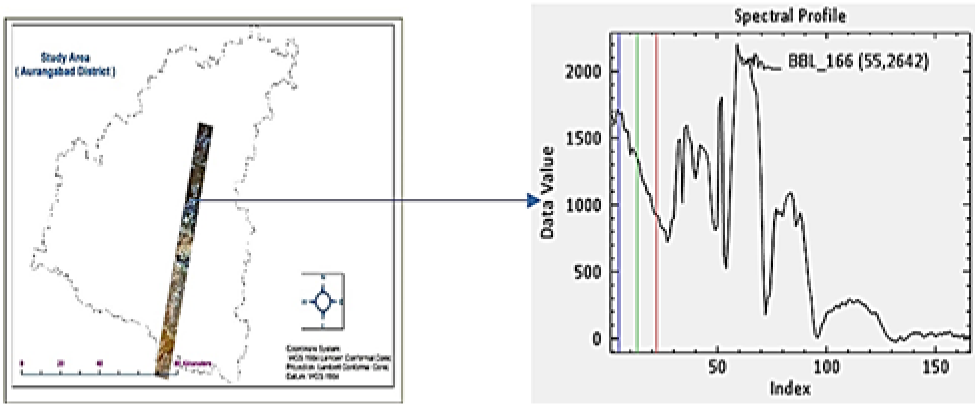

FIGURE. 5. AFTER REMOVING THE BAD BANDS AND ITS SPECTRAL PLOT

B. Destriping

Local destriping techniques are used to eliminate the vertical stripes. They are highly suggested for vertical stripe removal since they only affect the strip column layer. The vertical strips removed procedure improves the connection between reflection spectra and mineral spectra and aids in mineral classification formulation precision. Pour, A. B., and M. Hashim (2014). Table 3 displays the availability of vertical strips in the images column. Figure 6 depicts the spectral profile plot and visualisation variation after the vertical strips have been removed.

TABLE III. LIST OF VERTICAL STRIPS IN HYPERION (EO-1) IMAGERY

Sr. No.	Bands Number	Column Numbers	Sr. No.	Bands Number	Column Number
1	8,9	6,68,114,245	9	118	145

2	10,11	6,68,114	10	135	60
3	12	6	11	158	18
4	28,29	47	12	162	103
5	87,88	54	13	168	117
6	94	92	14	198	117
7	99	91	15	202	182
8	116	137	16	201	7

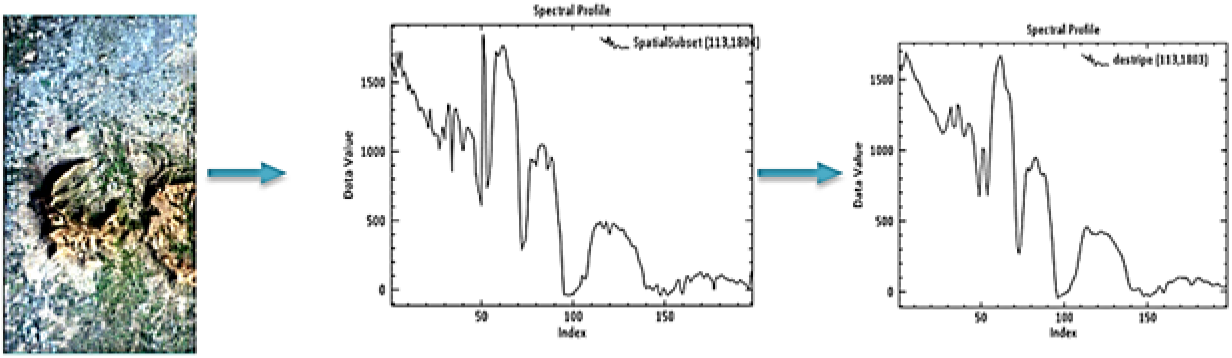

FIGURE. 6. EFFECT OF DESTRIPING IN VISUAL INTERPRETATION AND ITS SPECTRAL PLOT

C. Radiometric calibration

To determine the radiance value of the earth's surface, the radiometric calibration uses the DN value of Hyperion (EO-1) data. The output file format is BIL, with a scale factor of 0.1. (Pixel Interleaved Band) It converts digital numbers from the Hyperion (EO-1) CCD into radiance values. C. Zhang (2014). Figure 7 depicts the radiance value as well as its spectral profile plot.

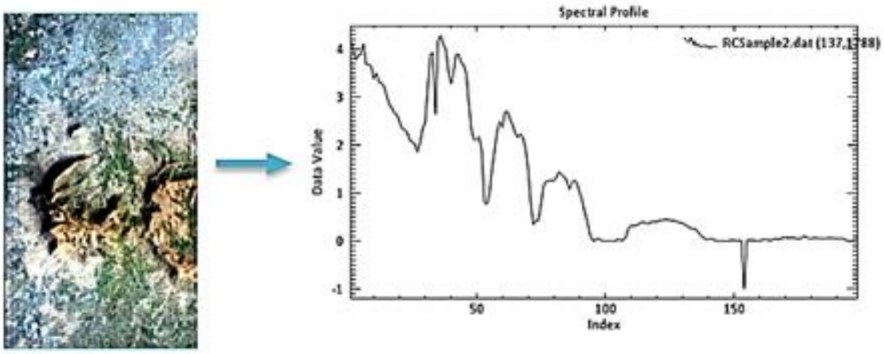

FIGURE. 7. RADIOMETRIC CALIBRATION AND ITS SPECTRAL PLOT

The FLAASH module is used to do atmospheric adjustment. FLAASH utilises sophisticated techniques to deal with the most difficult climatic circumstances, such as cloud cover. As an input image, FLAASH requires a radiometric calibrated radiance image in BIL format. Kumar, M. V., and K. Yarrakula's 4-byte signed numerals (2017). Figure 8 depicts the reflectance value and spectral profile plotted with the FLAASH module.

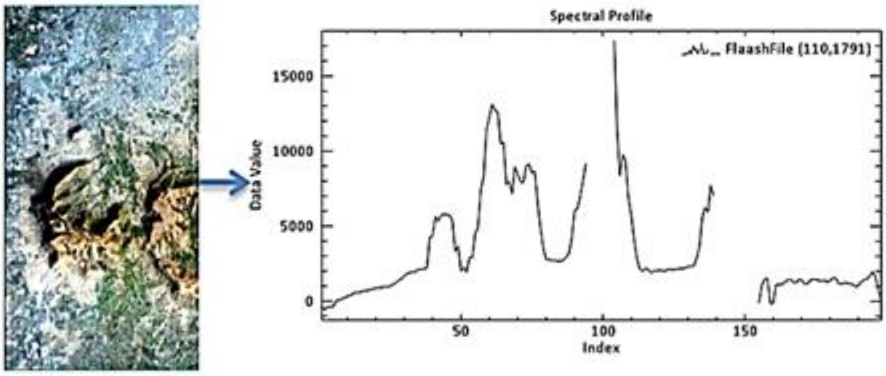

FIGURE. 8. FLAASH MODULE AND ITS SPECTRAL PLOT

D. Atmospheric correction module

The FLAASH module is used to do atmospheric adjustment. FLAASH utilises sophisticated techniques to deal with the most difficult climatic circumstances, such as cloud cover. As an input image, FLAASH requires a radiometric calibrated radiance image in BIL format. 4-byte signed numerals (2017). Figure 8 depicts the reflectance value and spectral profile plotted with the FLAASH module.

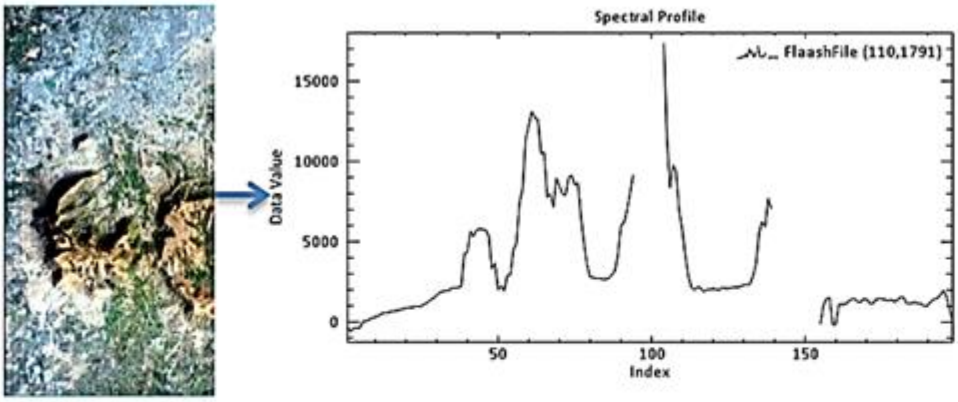

FIGURE. 9. FLAASH MODULE AND ITS SPECTRAL PLOT

E. Minimum Noise Fraction (MNF)

There is a lot of noise information in the reflectance bands of Hyperion (EO-1) imagery. The MNF transformation is a more advanced PCA algorithm. Depending on the amount of noise, MNF shortens the reflectance bands in ascending order. Kempeneers, P., et. al.(2004). Figure 9 clearly shows the large amount of noise present in the data and it affect the descending order bands. MNF takes only 9 bands in the region to process the Hyperion (EO-1) data.

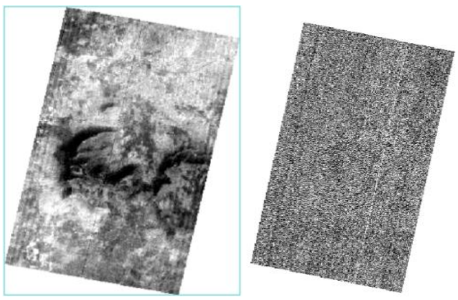

Band 6 Band 15

F. Pixel Purity Index(PPI)

MNG's noiseless bands are used as the pixel purity index input. PPI processes the MNF bands in iterations ranging from 2.5 to 10000. In the PPI, impure and pure pixels are represented by black and white pixels, respectively, Upadhyay, M. R. (2013). Figure 10 depicts the image's pixel purity index.

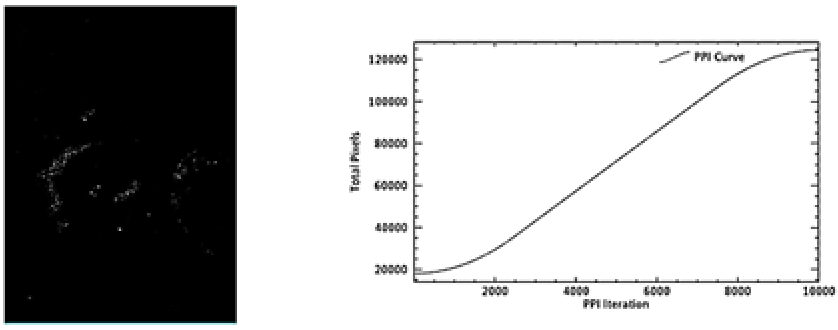

FIGURE. 10. PIXEL PURITY INDEX.

G. Spectral Analysis

The spectral libraries of the USGS and NASA were used to get the Alunite mineral spectra. These mineral spectra have a band interval of 2.5nm, whereas the Hyperion (EO-1) imaging spectra have a band interval of 10nm. Spectral Resembling techniques are used to transform library spectra data from 2.5nm to 10nm intervals. The spectral analyzer programme compares Alunite mineral spectra to picture spectra and provides probability estimates using methods such as SAM, SFF, and BE. In this study, Alunite mineral has a high probability of approximately 0.85 in the wavelength range between 2000nm and 2500nm.

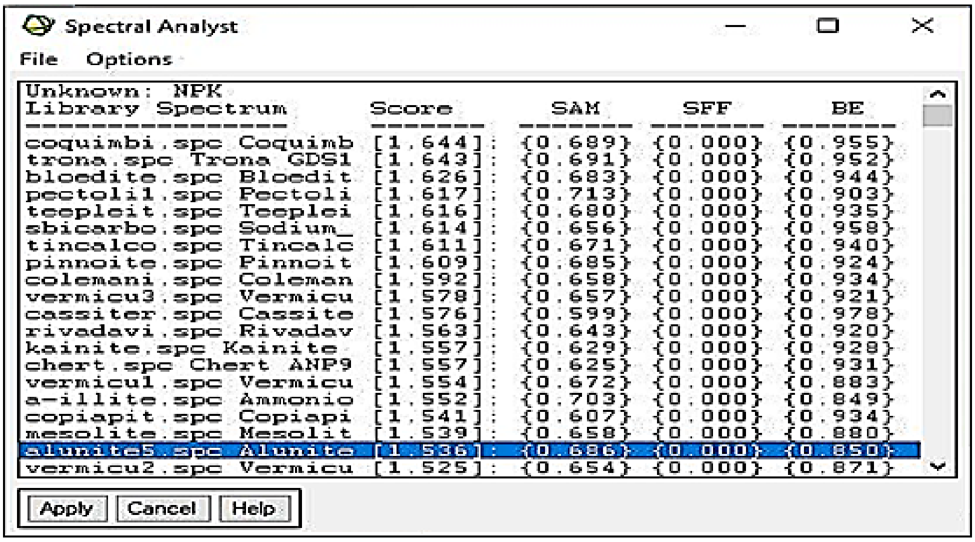

Spectral Analyst

File Options

Unknown: NPK

Library Spectrum	Score	SAM	SFF	BE
coquimbi.spc Coquimb	[1.644]:	{0.689}	{0.000}	{0.955}
trona.spc Trona GDS1	[1.643]:	{0.691}	{0.000}	{0.952}
bloedite.spc Bloedit	[1.626]:	{0.683}	{0.000}	{0.944}
pectolil.spc Pectoli	[1.617]:	{0.713}	{0.000}	{0.903}
teepleit.spc Teeplei	[1.616]:	{0.680}	{0.000}	{0.935}
sbicarbo.spc Sodium_	[1.614]:	{0.656}	{0.000}	{0.958}
tincalco.spc Tincalc	[1.611]:	{0.671}	{0.000}	{0.940}
pinnoite.spc Pinnoit	[1.609]:	{0.685}	{0.000}	{0.924}
colemani.spc Coleman	[1.592]:	{0.658}	{0.000}	{0.934}
vermicu3.spc Vermicu	[1.578]:	{0.657}	{0.000}	{0.921}
cassiter.spc Cassite	[1.576]:	{0.599}	{0.000}	{0.978}
rivadavi.spc Rivadav	[1.563]:	{0.643}	{0.000}	{0.920}
kainite.spc Kainite	[1.557]:	{0.629}	{0.000}	{0.928}
chert.spc Chert ANP9	[1.557]:	{0.625}	{0.000}	{0.931}
vermicul.spc Vermicu	[1.554]:	{0.672}	{0.000}	{0.883}
a-illite.spc Ammonio	[1.552]:	{0.703}	{0.000}	{0.849}
copiapit.spc Copiapi	[1.541]:	{0.607}	{0.000}	{0.934}
mesolite.spc Mesolit	[1.539]:	{0.658}	{0.000}	{0.880}
alunite5.spc Alunite	[1.536]:	{0.686}	{0.000}	{0.850}
vermicu2.spc Vermicu	[1.525]:	{0.654}	{0.000}	{0.871}

Apply Cancel Help

FIGURE. 11. ALUNITE MINERAL PROBABILITY

Figure 11 depicts the total likelihood score obtained when comparing picture spectra to mineral spectra. Figure 12 depicts the relationship between picture spectra and mineral spectra. The white line represents the mineral spectrum of the endmember. The picture spectra were represented by the red line.

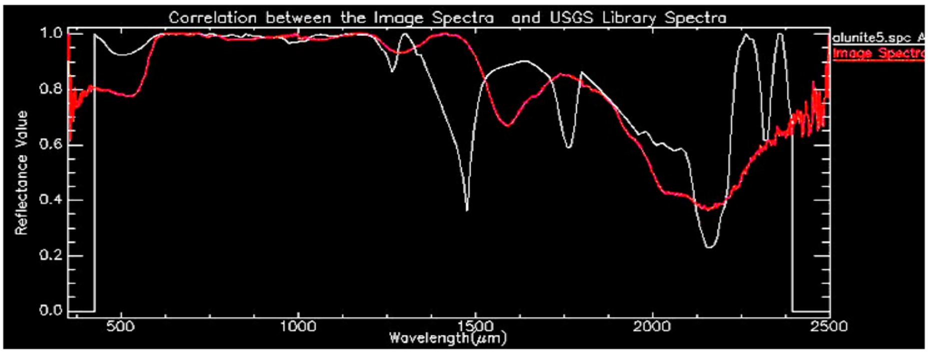

FIGURE. 12. IMAGE SPECTRA AND LIBRARY SPECTRA ARE CORRELATED.

H. Spectral Angle Mapper

In the spectral angle mapper technique, the image spectrum and Alunite spectra are compared. The bands in the SWIR area extend from 1900nm to 2400nm. The angle between the picture and the endmember mineral spectra is 0.25 degrees. The existence of the Alunite mineral in the earth's topography is shown by the red pixels in the SAM result. In Figure 13, the Alunite material is classified using SAM. The dark pixels represent other earth surface things that inhabit the region. In the Aurangabad district.

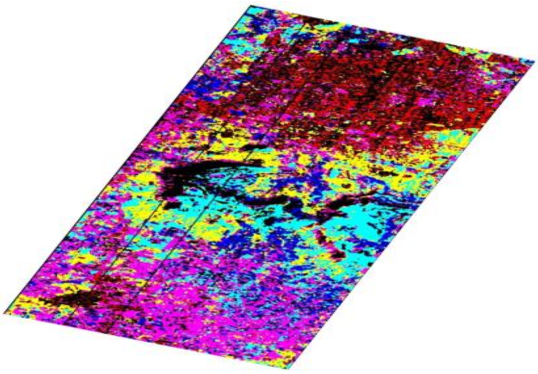

FIGURE. 13. ALUNITE MINERAL IDENTIFICATION USING THE SPECTRAL ANGLE MAPPER

V. CONCLUSION

The goal of this research was to see if Hyperion (EO-1) data could be used to quantify and map the mineral potential zone. It analyses hyperspectral data and compares the results to the research area's field spectra and geological map. It demonstrates how the Hyperion data can be used to map geological properties and detect mineral abundance.

Hyperion imaging, on the other hand, has its own set of restrictions, including a low signal-to-noise ratio, the appearance of apparent strips in multiple bands, and limited spectral special resolution.

Based on past information about the area, a logical method of Hyperspectral remote sensing was use. It was successful in emphasizing the value of the mineral Alunite. The Spectral Angle Mapper method was use to map these targeted minerals using Hyperion data.

The spectra were matched using the composite score of SAM, SFF, and BE in this investigation. SAM was used to classify the minerals that scored well (>1.5). It has a strong correlation with the data collected in the field. The position, strength, and shape of the absorption feature of spectral curves were use to identify individual mineral species. Only the absorption characteristic in each spectrum is attempted to be match by the spectral curve matching approach. Fieldspec4 field sample is required for further verification.

VI. REFERENCES

[1]. Datt, B., McVicar, T. R., Van Niel, T. G., Jupp, D. L., & Pearlman, J. S. (2003). Preprocessing EO-1 Hyperion hyperspectral data to support the application of agricultural indexes. IEEE Transactions on Geoscience and Remote Sensing, 41(6), 1246-1259.

[2]. Dill, H. G. (2001). The geology of aluminium phosphates and sulphates of the alunite group minerals: a review. Earth-Science Reviews, 53(1-2), 35-93.

[3]. Gore, R., Mishra, A., & Deshmukh, R. (2020). Mineral Mapping at Lonar Crater Using Remote Sensing. Journal of Scientific Research, 64(2).

[4]. Kumar, M. V., & Yarrakula, K. (2017). Comparison of efficient techniques of hyper-spectral image preprocessing for mineralogy and vegetation studies.

[5]. Kempeneers, P., Deronde, B., Bertels, L., Debruyn, W., De Backer, S., & Scheunders, P. (2004, September). Classifying hyperspectral airborne imagery for vegetation survey along coastlines. In IGARSS 2004. 2004 IEEE International Geoscience and Remote Sensing Symposium (Vol. 2, pp. 1475-1478). IEEE.

[6]. Kokaly, R. F., Clark, R. N., Swayze, G. A., Livo, K. E., Hoefen, T. M., Pearson, N. C., ... & Klein, A. J. (2017). USGS spectral library version 7 (No. 1035). US Geological Survey.

[7]. Mahoney, J. J. (1988). Deccan traps. In Continental flood basalts (pp. 151-194). Springer, Dordrecht.

[8]. Middleton, E. M., Ungar, S. G., Mandl, D. J., Ong, L., Frye, S. W., Campbell, P. E., ... & Pollack, N. H. (2013). The earth observing one (EO-1) satellite mission: Over a decade in space. IEEE Journal of Selected Topics in Applied Earth Observations and Remote Sensing, 6(2), 243-256.

[9]. Pal, M. K., & Porwal, A. (2015, July). Destriping of Hyperion images using low-pass-filter and local-brightness-normalization. In 2015 IEEE International Geoscience and Remote Sensing Symposium (IGARSS) (pp. 3509-3512). IEEE.

[10]. Pour, A. B., & Hashim, M. (2014). ASTER, ALI and Hyperion sensors data for lithological mapping and ore minerals exploration. SpringerPlus, 3(1), 1-19.

[11]. Schneider, S., Murphy, R. J., & Melkumyan, A. (2014). Evaluating the performance of a new classifier–the GP-OAD: A comparison with existing methods for classifying rock type and mineralogy from hyperspectral imagery. ISPRS journal of photogrammetry and remote sensing, 98, 145-156.

[12]. Solutions, H. G. (2017). Fast line-of-sight atmospheric analysis of hypercubes (flaash). Accessed: Dec.

[13]. Upadhyay, M. R. (2013). Indian Space Research Organisation Department of Space Government of India Dehradun–248001 (Doctoral dissertation, Indian Institute of Remote Sensing).

[14]. Van Der Meer, F. (2004). Analysis of spectral absorption features in hyperspectral imagery. International journal of applied earth observation and geoinformation, 5(1), 55-68.

[15]. Vigneshkumar, M., & Yarakkula, K. (2017, November). Nontronite mineral identification in nilgiri hills of tamil nadu using hyperspectral remote sensing. In IOP Conference Series: Materials Science and Engineering (Vol. 263, No. 3, p. 032001). IOP Publishing.

[16]. Wyatt, C. (2012). Radiometric calibration: theory and methods. Elsevier.

[17]. Zhang, L., & Du, B. (2012). Recent advances in hyperspectral image processing. Geo-spatial Information Science, 15(3), 143-156.

[18]. Zhang, C. (2014). Combining hyperspectral and LiDAR data for vegetation mapping in the Florida Everglades. Photogrammetric Engineering & Remote Sensing, 80(8), 733-743.